DOI: 10.26599/FSHW.2025.9250825

Contents lists available at SciOpen

Food Science and Human Wellness

journal homepage: https://www.sciopen.com/journal/2097-0765

China Food Publishing Co.

A Pathophysiological Hepatocyte Senescence Model Mimicking Lipid Overload and Oxidative Stress via dietary OA/PA and H_2O_2 Co-Treatment

Xuan Jiang[a, b, †], Fengmin Xiong[a, †], Zhimou Guo[a, b], Bin Zhang[a], Xianlong Ye[a, *], Shenglong Zhu[c, *], Xinmiao Liang[a, b, d, *]

[a] *Ganjiang Chinese Medicine Innovation Center, Nanchang 330000, China.*

[b] *Dalian Institute of Chemical Physics, Chinese Academy of Sciences, Key Laboratory of Separation Science for Analytical Chemistry, Dalian 116023, China.*

[c] *Wuxi School of Medicine, Jiangnan University, Wuxi, China.*

[d] *State Key Laboratory of Phytochemistry and Natural Medicines, Dalian 116023, China.*

ABSTRACT: Alleviating hepatocyte senescence offers potential for treating chronic liver diseases. However, current models of hepatocyte senescence fail to recapitulate the multifactorial pathology of aged livers, primarily relying on oxidative stress induction that produces oversimplified phenotypes. To address this issue, integrative transcriptomic and fatty acid determination of aged murine liver tissues revealed profound dysregulation of fatty acid metabolism, characterized by pathological accumulation of diet-related fatty acids oleic acid (OA) and palmitic acid (PA). We developed a physiomimetic senescence induction paradigm combining OA/PA with hydrogen peroxide (H_2O_2) exposure across four human and murine hepatic cell systems. This dual-hit approach generated more prominent senescence hallmarks, including senescence-associated β-galactosidase activity, lipid droplet formation, redox imbalance, and cell cycle arrest. Transcriptomic analysis revealed enhanced aging hallmark genes regulation in THLE-2 cells cotreated with OA/PA and H_2O_2 than in those treated with H_2O_2 alone. Crucially, the anti-aging drug rapamycin reversed senescence phenotypes and lipid accumulation exclusively in the dual-induction model, validating its pathophysiological relevance. Our work establishes aberrant lipid metabolism as an essential accelerator of hepatocyte senescence. A fatty acid-rich environment mimicking high-lipid dietary conditions combined with H_2O_2 exposure induces hepatocytes resembling aged livers, and this updated hepatocyte senescence model provides an advanced tool for screening dietary interventions or functional foods targeting age-related liver disorders.

Keywords: Liver senescence, aging model, H_2O_2, OA, PA

1. Introduction

Chronic liver diseases (CLDs) have emerged as a leading source of morbidity and mortality globally, accounting for 2 million deaths[1]. The prevalence of CLD has increased notably in recent years[2]. Most CLDs encompass nonalcoholic fatty liver disease (NAFLD), with hepatitis B virus (HBV), hepatitis C virus (HCV), and alcoholic liver disease following[3-5]. Evidence indicates that aging is a critical factor contributing to the

† These authors contributed equally to this work.
***Corresponding author**
shenglongzhu@jiangnan.edu.cn, yexianlong@jcmsc.cn, liangxm@dicp.ac.cn

Received 22 April 2025
Received in revised from 26 May 2025
Accepted 25 July 2025

increased incidence of chronic liver diseases, particularly NAFLD and nonalcoholic steatohepatitis (NASH)[6]. Aging not only exacerbates the prognosis of these conditions but also serves as the predominant risk factor for their development across various stages[7]. Senescent hepatocytes, characterized by elevated fat deposition, inflammation, extracellular matrix (ECM) production, and fibrosis, play pivotal roles in the pathogenesis of CLDs. Furthermore, increasing evidence suggests that senescent hepatocytes could be therapeutically targeted in NAFLD to reduce insulin resistance (IR), steatosis, and fibrosis[8]. As a vital endocrine organ, the aging liver may significantly impact the health of other organs. Therefore, the development of interventions for liver aging, which favor the prevention and alleviation of liver aging-related diseases, especially CLDs, is promising and urgently needed. For example, FGF21 beneficially modulates liver metabolism as a longevity-promoting hormone[9, 10]. The potent anti-aging drugs rapamycin and metformin have modest effects on hepatic lipidosis[11, 12]. This finding suggests that reducing the appearance of liver aging characteristics may indeed lower the incidence of CLDs, highlighting the potential therapeutic benefits of targeting liver aging.

The development of stable and effective cell models for studying senescence has facilitated the exploration of its physiological and pathological roles and the evaluation of senescent hepatocytes as therapeutic targets[13]. However, the lack of specific and broadly applicable cell models makes it difficult to accurately identify and characterize the key genes and signaling pathways that drive liver senescence. Research has shown that abnormal lipid metabolism accelerates hepatic cell senescence [14, 15] and that lipid accumulation is considered a hallmark of liver aging. Prior cell models have induced senescence through oxidative stress, gamma irradiation, UVB irradiation, or oncogene overexpression[16-19]. However, these models have limitations as different cell types respond variably to a given stressor[20]. To simulate the diverse phenotypes of liver aging observed *in vivo*, particularly lipid accumulation and cell senescence, it is imperative to develop more comprehensive and physiologically relevant models.

This study examined liver pathology in two aging mouse models and identified abnormal fatty acid metabolism as a key feature of liver aging, with the aid of transcriptomics and fatty acid composition analysis. On the basis of these findings, we constructed a novel model of hepatocyte aging by supplementing the H_2O_2-induced hepatocyte model with a mixture of two fatty acids that significantly accumulate with age. This model successfully simulates various markers of cell senescence, including lipid metabolism disorders and alterations in oxidative stress levels. Transcriptomic analysis revealed that more aging hallmark genes were regulated by treatment with OA/PA combined with H_2O_2. Furthermore, we evaluated the lipid-lowering and anti-aging effects of rapamycin in this model.

This study provides a model that can comprehensively simulate the aging phenotype and cause more significant changes in indicators, facilitating the discovery of effective anti-aging drugs and increasing the hit rate of drugs with anti-aging effects in the drug screening process.

2. Materials and methods

2.1 Cell culture

The hepatic cells were sourced from ATCC. Cells were cultured in specific media and incubated at 37℃ in a humidified atmosphere with 5% CO_2. BNL CL.2 and HepG2 cells were grown in DMEM (Gibco, USA, C11995500BT) with 1% streptomycin and penicillin (Solarbio, China, P1400) and 10% fetal bovine serum (PAN, Germany, ST30-3302). THLE-2 cells were grown in DMEM/F12 (Gibco, USA, C11330500BT) with 15% fetal bovine serum and 1% streptomycin-penicillin. AML12 cells were cultured in complete DMEM/F12 medium with 10% fetal bovine serum, 1 × ITS (Beyotime, China, C0341), 40 ng/mL dexamethasone (Sangon Biotech, China, A601187), and 1 × streptomycin and penicillin.

2.2 Cell treatment with H2O2 and OA/PA

Upon reaching 70%–80% confluence, cells were exposed for 24 hours to varying concentrations of H_2O_2, oleic acid/palmitic acid (OA/PA, molar ratio 2:1), or a combination of H_2O_2 and OA/PA. The specific concentrations of OA/PA (0.00–0.80 mmol/L) and H_2O_2 (0.00–2.00 mmol/L) used for the cell viability assay are detailed in **Tables S1–3**. To study the changes in senescence-related markers, the cells were treated as follows: 0.75 mmol/L OA/PA and 0.90 mmol/L H_2O_2 for HepG2 cells, 0.25 mmol/L OA/PA and 0.20 mmol/L H_2O_2 for THLE-2 cells, 0.20 mmol/L OA/PA and 0.10 mmol/L H_2O_2 for AML12 cells, and 0.50 mmol/L OA/PA and 1.00 mmol/L H_2O_2 for BNL CL.2 cells.

In the cell viability study, THLE-2 cells were exposed to varying concentrations of rapamycin (1, 2, 4, or 8 μmol/L) concurrently with 0.30 mmol/L H_2O_2 or a combination of 0.25 mmol/L OA/PA and 0.30 mmol/L H_2O_2. In other experiments, THLE-2 cells were treated with 2 μmol/L rapamycin concurrently with H_2O_2 or OA/PA + H_2O_2.

2.3 Cell viability assay

Cell viability was assessed post-induction using the Cell Counting Kit-8 (CCK-8, Meilunbio, China, MA0225) following the manufacturer's guidelines. A colorimetric reading was taken at 450 nm. The percentage of viable cells was calculated from the optical density and normalized to the values of the controls.

2.4 Senescence-associated β-galactosidase (SA-β-gal) activity assay

The SA-β-gal activity assay was performed via a β-gal activity assay kit (Solarbio, China, BC2585). β-gal decomposes p-nitrobenzene-β-D-galactoside pyranopyranoside to p-nitrophenol, which exhibits a maximum absorption peak at 400 nm. β-gal activity was calculated by measuring the rate of increase in the absorption value.

2.5 SPiDER-β-galactosidase assay

The cells were washed with HBSS (Solarbio, China, H1146), and fixed with 4% paraformaldehyde/PBS for 3 minutes at room temperature. Cells were washed three times with HBSS, followed by the addition of SPiDER-β-Gal working solution (DOJINDO LABORATORIES, Japan, SG03) to the culture plates for 30 minutes at 37℃ without CO_2. After the reaction, the cells were washed with

HBSS. SA-β-gal-positive cells were imaged using a fluorescence microscope with 488 nm excitation and 533 nm emission wavelengths.

2.6 Quantitative real-time PCR (qRT-PCR)

Total RNA was extracted via TRIzol reagent (Admas Life, China, G8011) and reverse transcribed into cDNA via StarScript III All-in-One RT Mix with gDNA Remover (Genestar, China, A230) according to the manufacturer's protocols. We used 2 × RealStar Fast SYBR qPCR Mix (Genestar, China, A304), with actin serving as the endogenous normalization control. Gene expression levels were calculated via the $2^{-\Delta\Delta Ct}$ method. The primers used in the study are shown in **Table S4**.

2.7 Flow Cytometry

The cells were collected and washed twice with cold PBS. The cells were then fixed with 75% ethanol for 4 h at 4℃. Two more washes were conducted following centrifugation to obtain the cell pellets. A total of 400 μL of 50 μg/mL PI and 100 μL of 100 μg/mL RNaseA (BD Biosciences, USA, 550825) were applied to the cells for 15 min. The cell cycle was detected via flow cytometry (BD Biosciences, USA, BD LSRFortessa™) and analyzed via FlowJo.

2.8 RNA-seq

Cellular RNA was extracted via a TRIzol reagent kit (Invitrogen, USA, 12183555). RNA quality was evaluated using an Agilent 2100 Bioanalyzer (Agilent Technologies, Palo Alto, CA, USA) and confirmed by RNase-free agarose gel electrophoresis. RNA-seq was conducted by Gene Denovo Biotechnology (Guangzhou, China) using the Illumina NovaSeq 6000 platform following cDNA library preparation. Gene expression levels was normalized to the fragments per kilobase of transcript per million mapped reads (FPKM) value. DEGs between groups were identified using a cutoff of $P < 0.05$ and an absolute log-transformed fold change ($|FC| \geq 2$. RNA-Seq data were statistically analyzed using OmicShare and visualized with Hiplot. To identify aging-related genes, we compare the differentially expressed genes (DEGs) identified through transcriptomic analysis with established aging-related databases, including the Aging Atlas, GeneCards, the Human Ageing Genomic Resources (HAGR), and the Online Mendelian Inheritance in Man (OMIM).

2.9 Animal studies

The animal experiment pro tocol was approved by the Animal Ethics Committee of by Laboratory Animal Ethics Committee of Kangtai Medical Laboratory Services Hebei Co. Ltd. (MDL2023-09-28-04). C57BL/6 mice were obtained from SPF Biotechnology Co., Ltd. (Beijing, China). For the aging experiments, 3- and 24-month-old male mice (n=5 per group) were used. The mice were kept at (24 ± 2)℃ with 30% relative humidity on a 12-hour light/dark cycle, with unrestricted access to standard pellet food and water. D-galactose-induced senescent mouse models were constructed, and 9-week-old male mice (n=6 per group) received subcutaneous injections of D-galactose (D-gal) at a dosage of 300 mg/kg/day for 8

weeks. The mice were humanely euthanized, and the liver tissue was collected, weighed, and stored at -80℃ until further analysis.

2.10 Biochemical analysis

The total superoxide dismutase (SOD, A001-3-2), malondialdehyde (MDA, A003-1-2), cholesterol (TC, A111-1-1), triglyceride (TG, A110-1-1), alanine aminotransferase (ALT, C009-2-1), and aspartate aminotransferase (AST, C010-2-1) contents of the cells and liver tissues were determined by corresponding kits from Nanjing Jiancheng Bioengineering Institute (Nanjing, China). The protein concentration in the cells and liver tissues was determined via a BCA kit (Beyotime, China, P0010).

2.11 Hematoxylin and eosin (H&E) staining

Fresh liver tissues were collected, fixed in 4% paraformaldehyde for a minimum of 24 hours, and embedded in paraffin. Paraffin sections of liver tissues were stained via a standard H&E protocol. The H&E-stained images were recorded via a digital slide scanner (3D D HISTECH Ltd., Budapest, Hungary).

2.12 Oil red O staining

The working oil red O solution was obtained by diluting 0.5% (w/v) oil red O (Sigma, USA, O0625) dissolved in isopropanol at 3:2 with distilled water. The cells were washed twice with PBS and then fixed with 4% paraformaldehyde for 15 min. Then, the cells and tissue sections were washed with water and incubated in 60% isopropanol for 30 s. The samples were incubated in Oil Red O staining solution in the dark for 20 min at room temperature. The cells were counterstained with hematoxylin for 1 min, washed twice, and photographed via a light microscope (Nikon, Japan, Ts2). Quantification was performed using ImageJ software (NIH). For each sample, five randomly selected microscopic fields were analyzed. The lipid-positive area (red staining) was measured and expressed as a percentage of the total tissue area.

2.13 Fatty acid analysis

The fatty acid composition was determined via gas chromatography–mass spectrometry (GC–MS) as previously described[21]. In brief, total fatty acids in liver tissues were extracted via chloroform. The fatty acid methyl esters were produced and detected via a Q Exactive GC Orbitrap GC–MS/MS high-resolution mass spectrometer (Trace1300, Thermo Fisher Scientific, Waltham, MA, USA). A capillary column of an Rtx Wax column (30.0 m × 0.25 mm, Restek, Bellefonte, PA, USA) was utilized. All fatty acid peaks were detected within approximately 35 min. The retention times of fatty acid methyl ester standards (Sigma–Aldrich, USA) and Xcalibur acquisition software (version 4.0, Thermo Fisher Scientific, USA) were used to identify the peaks. An internal standard, pentadecanoic acid (C15:0), was utilized to compute the percentage makeup of each fatty acid.

2.14 Statistical analysis

Statistical analysis was performed via GraphPad Prism 9.0 software. Unpaired, two-tailed t-tests, one-way ANOVA, or two-way ANOVA were used for statistical analysis. Data are expressed as means ± SDs. Significance levels: $*P < 0.05$, $**P < 0.01$, $***P < 0.001$.

3. Results

3.1 Decreased liver function and increased lipid accumulation are accompanied by the aging process

Naturally aged mice and D-galactose-induced senescent mice were utilized to systematically elucidate the pathological features of aging. **Figure 1A** presents a schematic diagram illustrating the experimental process and techniques employed in the animal experiments. Old mice (24 months) exhibited significant increases in body and liver weight compared to young mice (3 months) ($P < 0.01$). Conversely, D-galactose-induced senescent mice showed decreases in these parameters relative to normal mice ($P < 0.001$, $P < 0.01$), as depicted in **Figure 1B and 1C**. In both Models 1 and 2, aged mice exhibited increased levels of TC, TG, ALT, and AST in liver tissues ($P < 0.05$, $P < 0.01$, $P < 0.001$), except for the TC content in naturally aged mice, which remained comparable to that of young mice. For liver oxidative stress indicators, both aging model mice showed a significant increase in liver MDA content and a decrease in SOD content. Liver histology was performed via H&E and Oil Red O staining. Histological examination of the livers revealed prominent lipid droplets in the hepatocytes of the old mice and D-gal-treated mice, unlike those in young or normal mice (**Fig 1D, E**).

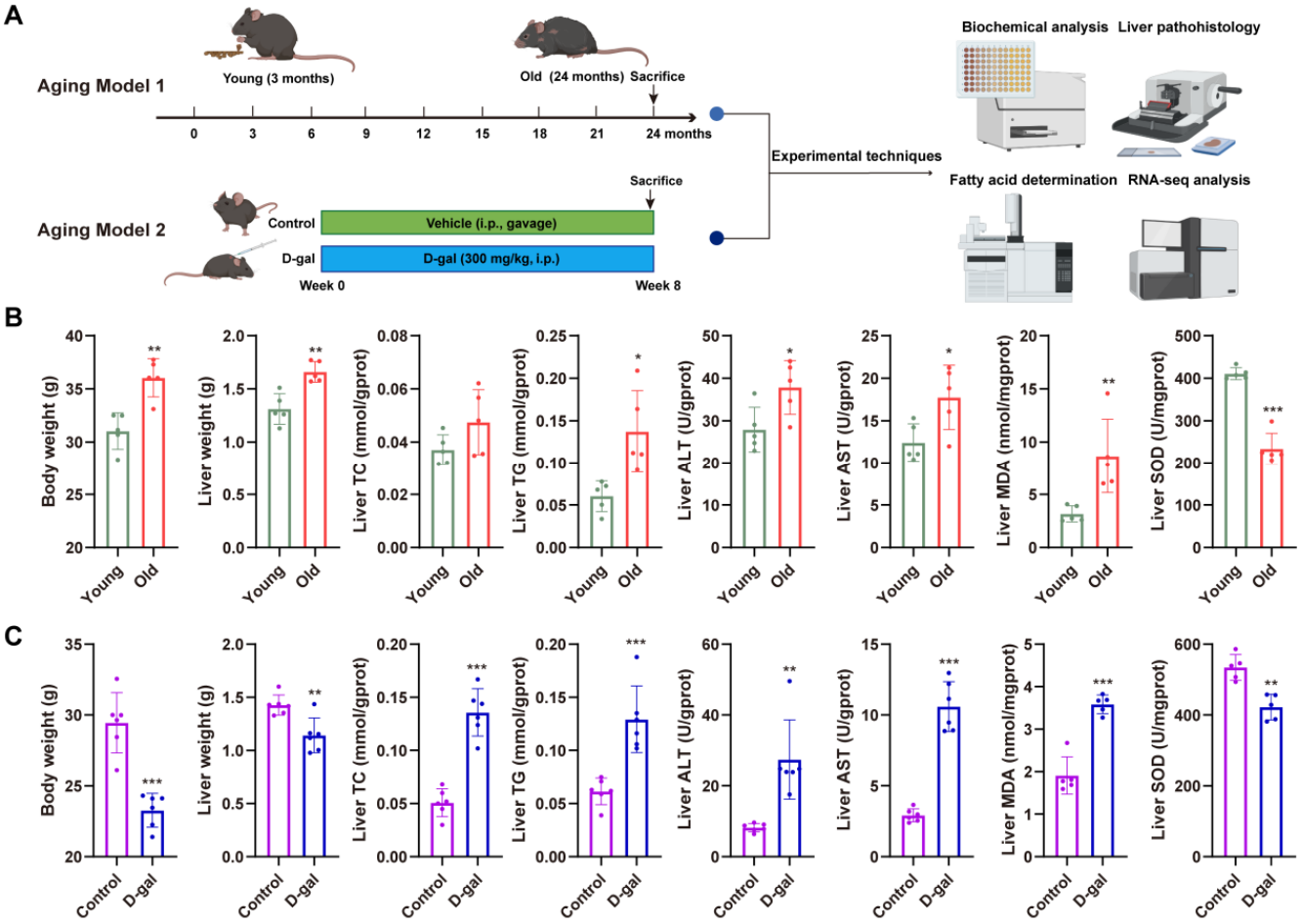

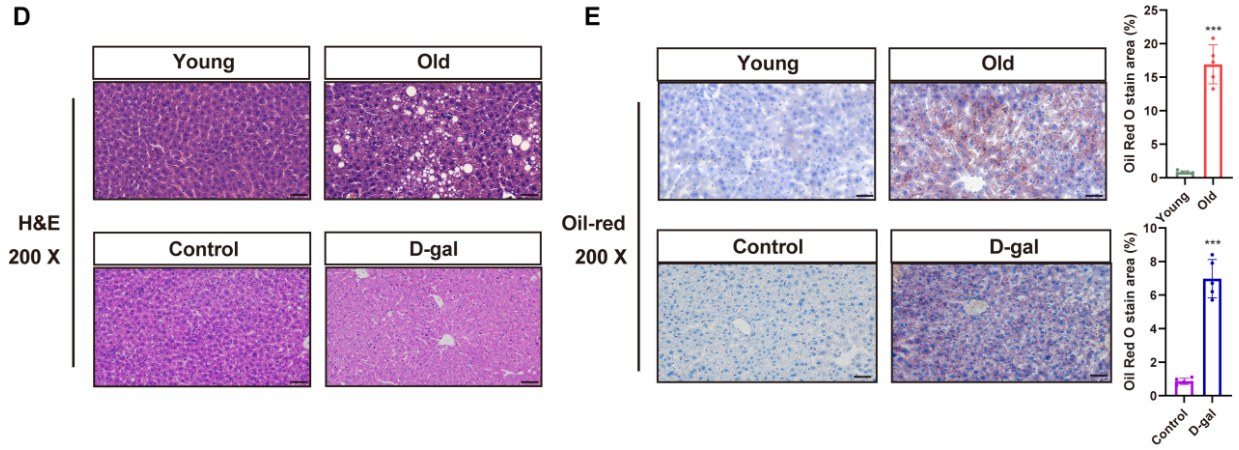

Fig 1. Body weight, liver biochemical indexes, and histological characteristics of two aging mouse models. (A) Schematic representation of the animal experiment. (B) The body weight, liver weight, and liver TC, TG, ALT, AST, SOD and MDA contents of the young mice (3 months) and the old mice (24 months). (C) The body weight, liver weight, and liver TC, TG, ALT, AST, SOD and MDA contents of the normal mice and the D-gal-injected mice. (D) Liver slices of two aging mouse models stained with hematoxylin and eosin (H&E, 200 X). (E) Liver slices of two aging mouse models stained with Oil red O (200 X) and quantified. N=5 or 6, $*p < 0.05$, $**P < 0.01$, $***P < 0.001$ determined by Dunnett's test following a one-way ANOVA or Tukey's test following a two-way ANOVA.

3.2 Abnormal fatty acid metabolism is associated with hepatocyte aging

To gain insight into the pathogenesis of liver aging, transcriptomic analysis was performed on liver tissues from young and old mice. **Figure 2A** outlines the workflow of the transcriptomic analysis. Principal component analysis (PCA) was utilized to distinguish each experimental group, revealing a complete separation between the young and old mouse groups (**Fig 2B**). The volcano plot (**Fig 2C**) illustrates the results of the differentially expressed gene (DEG) analysis, which revealed more upregulated genes (771) than downregulated genes (26). Gene Ontology (GO) enrichment analysis was conducted on the upregulated differentially expressed genes, with the top 10 terms ranked by ratio displayed in **Figure 2D**. The fatty acid metabolic process ranked first, with several fatty acid or lipid metabolism-related pathways also enriched and highly ranked. **Figure 2E** presents a heatmap of the top 20 genes associated with the GO term "fatty acid metabolic process". Old mice exhibited a marked increase in the expression of genes related to fatty acid metabolism compared to young mice.

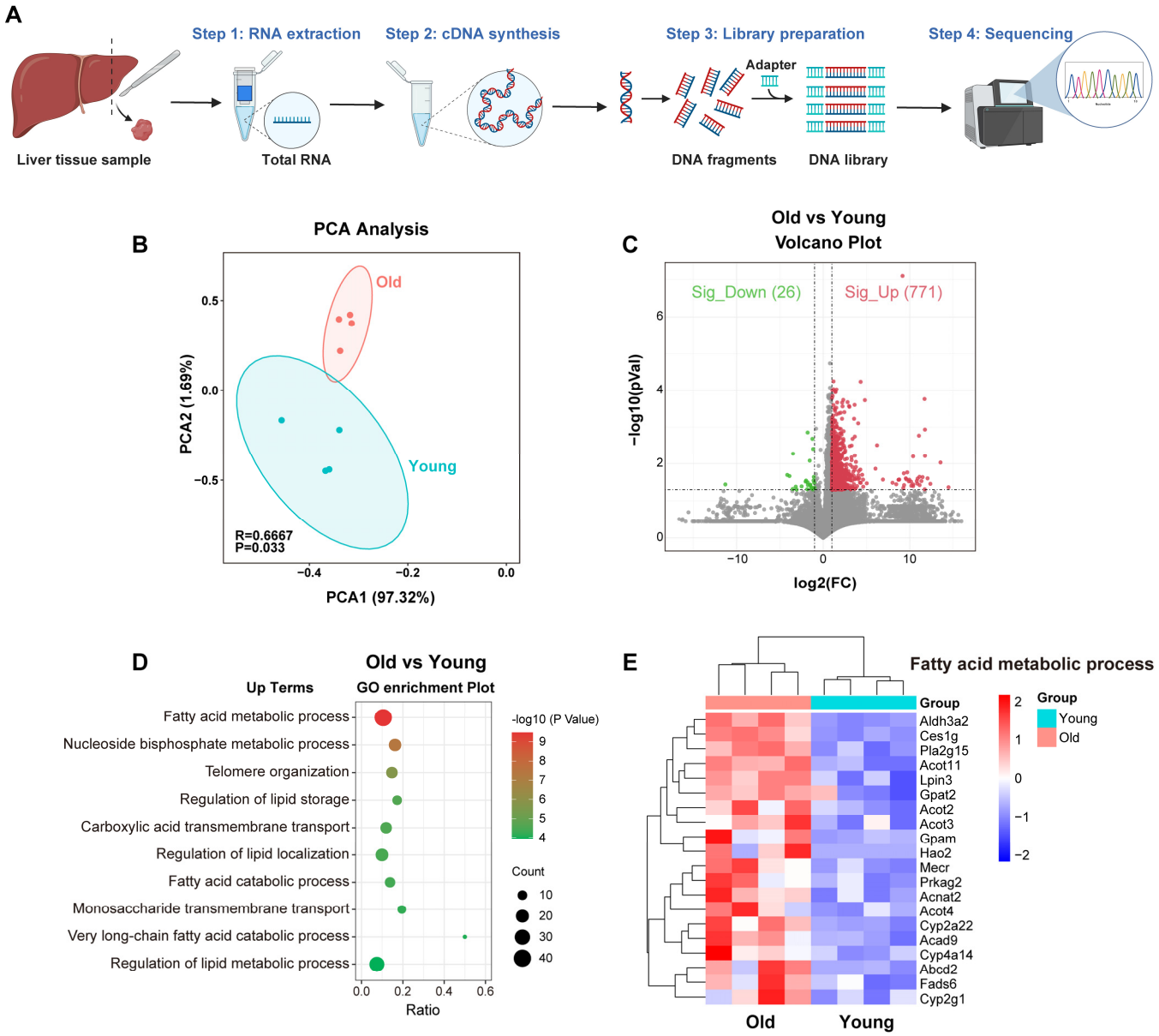

Fig 2. Transcriptome and fatty acid metabolism analysis of the livers of young and old mice. (A) Overview of the RNA-seq procedure. (B) The principal component analysis (PCA) of all genes in the liver between the young and old mice. (C) The differentially expressed genes (DEGs) between two groups. Green dots represent significantly downregulated DEGs, while red dots represent significantly upregulated DEGs. (D) GO enrichment analysis of upregulated DEGS between old and young mice. (E) Heat map of genes involved in the fatty acid metabolic process (TOP 20). N=4, *$p < 0.05$, ***$P <$ 0.001 determined by Dunnett's test following a one-way ANOVA.

3.3 Oleic acid and palmitic acid are significantly increased during hepatocyte aging

Transcriptomic analysis revealed a significant alteration in the fatty acid metabolism of the mouse liver with aging. The fatty acid composition of the mouse liver was subsequently investigated, as depicted in **Figure 3A**. Analysis of the fatty acid composition showed a significant increase in oleic acid (C18:1, OA), palmitic acid (C16:0, PA), and palmitoleic acid (C16:1) in the aged mice compared to young mice (**Fig 3B**). Oleic acid and palmitic acid were the two fatty acids with the greatest increases ($P < 0.01$). As shown in **Figure 3C,** data from the Human Aging and Longevity Landscape database (HALL) confirmed that oleic acid expression increased with age.

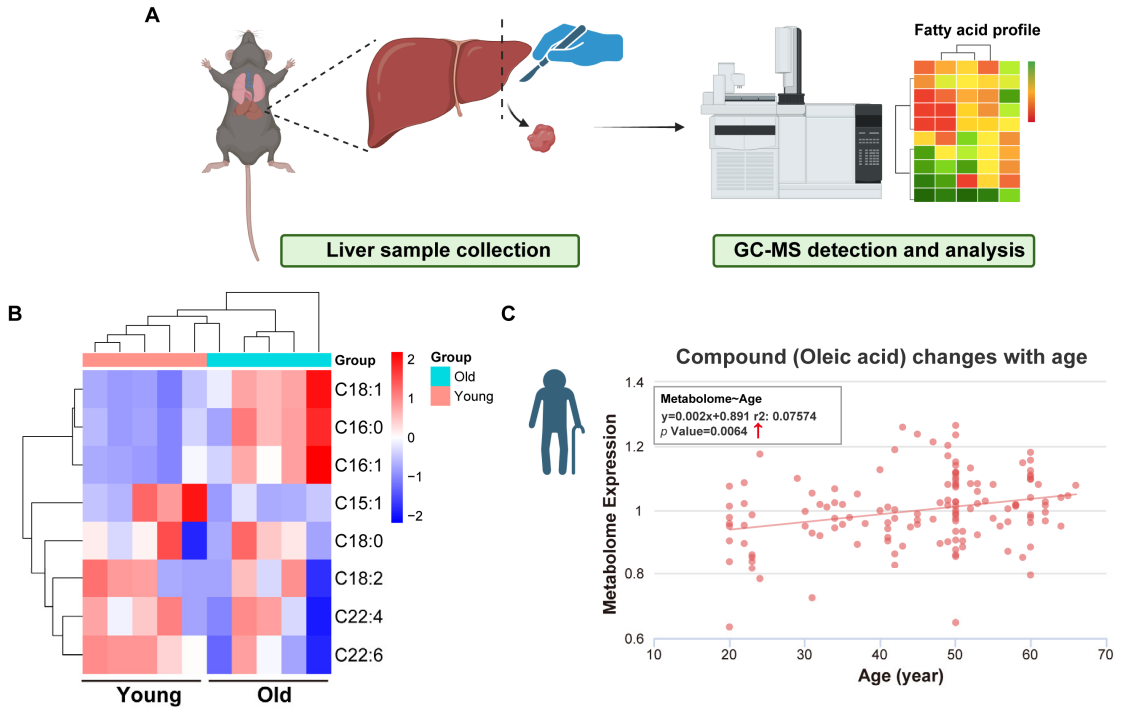

Fig 3. Transcriptome and fatty acid metabolism analysis of the livers of young and old mice. (A) Experiment schematic diagram of the determination and analysis of fatty acids in mouse liver. (B) Heat map of hepatic fatty acid composition. (C) Analysis of oleic acid expression in women of different ages, data from HALL database.

3.4 OA/PA combined with H_2O_2 induces senescence in hepatic cells

The top two age-related fatty acids were employed to establish a novel model of liver cell aging. Oleic acid and palmitic acid are frequently utilized to induce lipid accumulation or metabolic stress at a molar ratio of 2:1[22]. We utilized the CCK-8 assay to confirm the final concentrations of OA/PA (2:1) and H_2O_2 in AML12, BNL CL.2, HepG2, and THLE-2 cells (**Fig S1**). Senescence models of AML12 and THLE-2 cells were successfully constructed, demonstrating an increase in SPiDER-β-gal-positive cells and β-galactosidase activity (β-gal). Co-treatment of AML12 and THLE-2 cells with OA/PA and H_2O_2 significantly increased the relative fluorescence intensity of SPiDER-β-gal-positive cells compared to the control ($P < 0.01$, $P < 0.001$) and H_2O_2 groups ($P < 0.05$ for THLE-2) (**Fig 4A**), with consistent β-gal enzyme activity (**Fig 4B**). The impact of fatty acids on cells was assessed by measuring lipid droplet accumulation and TG content using Oil Red O staining and a TG detection kit. As shown in **Figure 4C and 4D**, there were no visible lipid droplets and no significant difference in TG content between the H_2O_2 group and the control group. Significant increases in intracellular TG content ($P < 0.001$) and numerous red lipid droplets were observed in both the OA/PA and OA/PA + H_2O_2 groups. Oxidative stress is crucial for senescence and aging[23]. Liver oxidative stress was assessed by quantifying MDA and SOD levels. In AML12 and THLE-2 cells, the combination of OA/PA and H_2O_2 led to decreased SOD activity and increased oxidative stress marker (MDA) (**Fig 4E**).

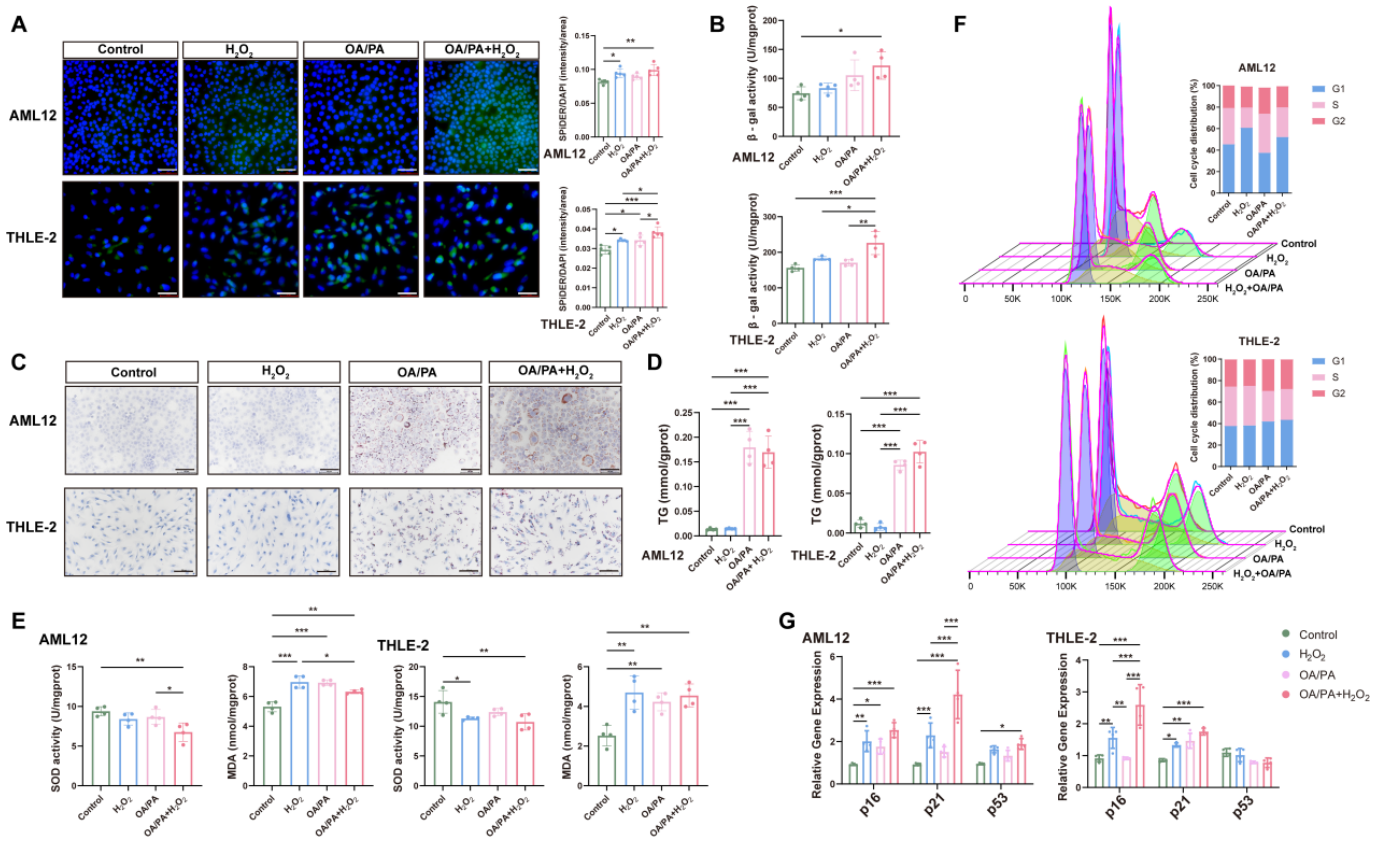

Fig 4. Senescence induction in hepatic cell lines AML12 and THLE-2 using H_2O_2 or OA/PA or H_2O_2 with OA/PA. (A) Representative images and quantification of SPiDER-β-Gal staining in AML12 and THLE-2 cells. Scale bar = 100 μm. (B) SA-β-Gal activity in AML12 and THLE-2 cells. (C) Representative Oil red O staining images of AML12 and THLE-2 cells. Scale bar = 100 μm. (D) TG levels in AML12 and THLE-2 cells. (E) SOD activity and MDA levels in AML12 and THLE-2 cells. (F) The cell cycle distribution of AML12 and THLE-2 cells was analyzed following treatments with H_2O_2 or OA/PA or a combination of H_2O_2 and OA/PA. (G) Relative gene expression level of p16, p21, and p53 in AM12 and THLE-2 cells treated with H_2O_2 or OA/PA or H_2O_2 with OA/PA. N=4, *p < 0.05, **P < 0.01, ***P < 0.001 determined by Dunnett's test following a one-way ANOVA or Tukey's test following a two-way ANOVA.

Flow cytometry quantified cells at each cell cycle stage based on the fluorescence intensity of propidium iodide-labeled DNA content. As shown in **Figure 4F**, compared with untreated cells, AML12 cells treated with H_2O_2 or OA/PA + H_2O_2 presented a marked increase in G1 phase cells (60.73%, 52.13%) and a decrease in S phase cells (19.00%, 27.75%), indicative of cell cycle arrest. The OA/PA group exhibited a reduced percentage of cells in the G1 phase. THLE-2 cells exhibited a similar cell cycle profile, showing a higher percentage of cells in the G1 phase in the OA/PA group compared to the OA/PA + H_2O_2 group (38.23%, P = 0.9877 and 43.48%, P = 0.0032, respectively), suggesting G1 phase arrest. Alterations in p16, p21, and p53 gene expression elucidate the mechanism of cell cycle arrest (**Fig 4G**). Gene expression analysis indicated significant upregulation of p16 and p21 in AML12 cells treated with H_2O_2 alone (P < 0.01, P < 0.01) or with both H_2O_2 and OA/PA (P < 0.001, P < 0.001). A significant increase in p53 expression was also observed in the OA/PA + H_2O_2 group of AML12 cells (P < 0.05). **Figure 4G** indicates that THLE-2 cells in the OA/PA + H_2O_2 group exhibited significantly higher gene expression levels of p16 and p21 compared to the control group (P < 0.001 for both). The H_2O_2 group exhibited significantly higher expression levels of p16 and p21 compared to the control group (P < 0.01, P < 0.05).

Experiments were similarly conducted in BNL CL.2 (murine embryonic liver cell line) and HepG2 (hepatocellular carcinoma cell line) cells (**Fig S2**). The fluorescence intensities for BNL CL.2 and HepG2 cells were similar when treated with OA/PA, H_2O_2, or their combination. Based on experimental results and the characteristics of the specific cell type, we concluded that BNL CL.2 and HepG2 cells are unsuitable for constructing a senescence model.

3.5 Transcriptomic analysis indicated that combined treatment induced more comprehensive aging-related gene alterations

Transcriptomic analysis was conducted to identify the DEGs between the control and OA/PA- and/or H_2O_2-treated THLE-2 cells. The volcano diagram shows that 101 (56 downregulated and 45 upregulated) and 578 (374 downregulated and 204 upregulated) DEGs responded to H_2O_2 or OA/PA with H_2O_2 treatment, respectively (**Fig 5A**). A total of 24 DEGs overlapped, as shown in the Venn diagram (**Fig 5B**). A total of 77 and 554 unique DEGs were identified in the H_2O_2 and OA/PA + H_2O_2 groups, respectively. All DEGs in the H_2O_2 and OA/PA + H_2O_2 groups were subsequently compared against 896 aging hallmark genes from four databases (Aging Atlas, GeneCards, HAGR, OMIM). Three DEGs (2.97% of 101) and 44 DEGs (7.61% of 578) were mapped to aging hallmark genes in the H_2O_2 and OA/PA + H_2O_2 groups, respectively (**Fig 5C**). In addition, GO enrichment analysis was performed. **Figure 5D** displays the top 10 pathways or GO-BP terms enriched by either up- or downregulated DEGs. The upregulated genes were predominantly enriched in GO terms associated with “cellular response to biotic stimulus”, “cellular response to lipid”, “positive regulation of response to external stimulus”, and “inflammatory response”. The enrichment of the negative regulation of the cell population proliferation pathway aligns with the slow cell proliferation observed during cell aging. The downregulated genes were enriched in GO pathways related to the innate immune response and the response to stimuli. In conclusion, transcriptome analysis and previous experiments showed that the induction of OA/PA plus H_2O_2 could more comprehensively simulate aging characteristics *in vivo*.

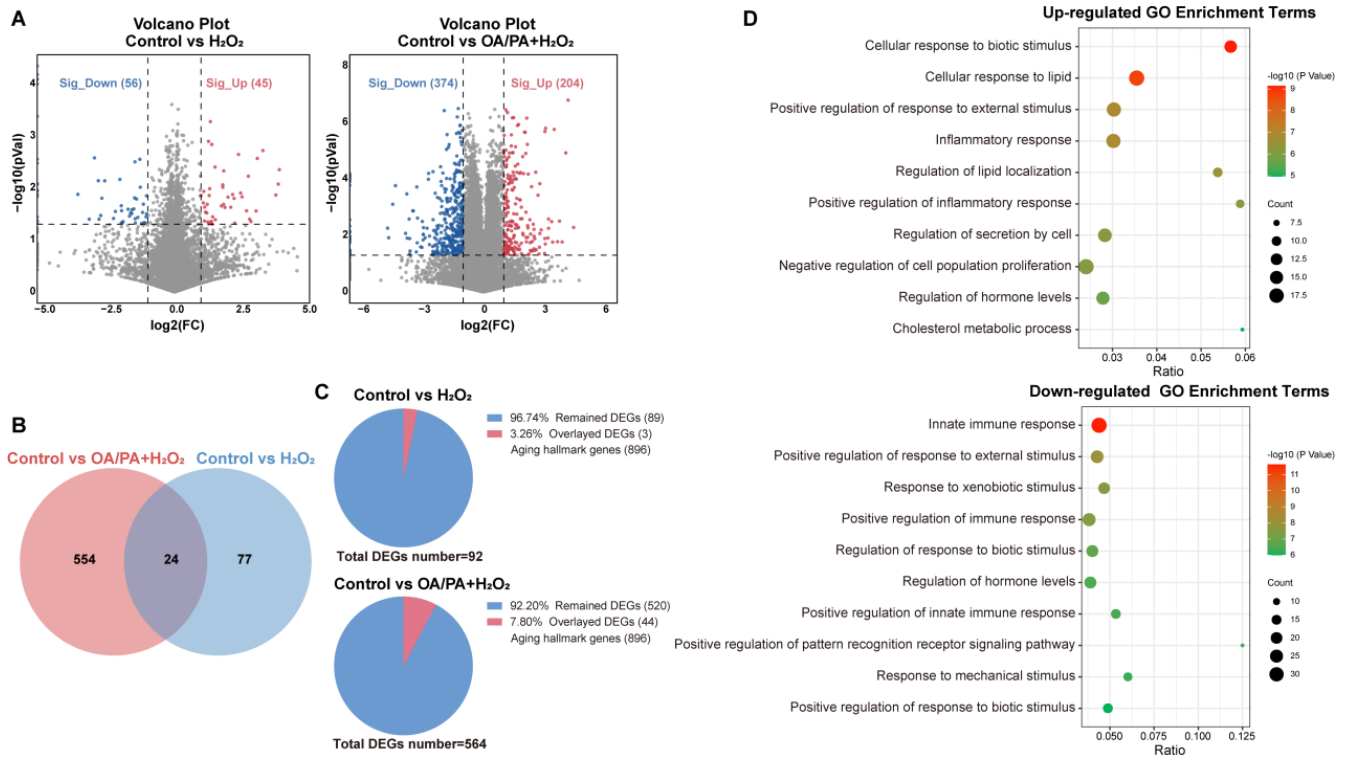

Fig 5. Transcriptome analysis of the THLE-2 cell treated with H_2O_2 or/and OA/PA. (A) Volcano plot of DEGs between the control group and H_2O_2 group or OA/PA + H_2O_2 group. (B) Venn diagrams of DEGs between the control group and H_2O_2 group or OA/PA + H_2O_2 group. (C) The proportion of DEGs and age-related genes in the aging database between the control group and H_2O_2 group or OA/PA + H_2O_2 group. (D) GO enrichment analysis of DEGs between the H_2O_2 group and OA/PA + H_2O_2 group.

3.6 Combined treatment-induced senescent model identified lipid-lowering and anti-aging effects of rapamycin synchronously

A crucial factor in assessing a new model is its ability to identify effective drugs during experiments. To validate the model, we induced senescence in THLE-2 cells with either H_2O_2 or OA/PA plus H_2O_2 while simultaneously treating them with varying concentrations of rapamycin. The final dose of rapamycin was determined to be 2 μmol/L on the basis of its modest cytotoxic impact on OA/PA- and H_2O_2-induced THLE-2 cells in the CCK-8 experiment (**Fig 6A**). **Figure 6B** (TG content detection) and **Figure 6C** (Oil red O staining) confirmed rapamycin's lipid-lowering effect, absent in H_2O_2-induced THLE-2 cells. The excellent lipid-lowering effect of rapamycin may contribute to its ability to delay cell senescence. In addition, H_2O_2-induced models performed worse than OA/PA and H_2O_2 co-induced cell models in evaluations of anti-aging. **Figure 6D** indicates no significant difference between the 2 μmol/L rapamycin group and the control group in H_2O_2-induced THLE-2cells, whereas the relative fluorescence intensity of SPiDER-β-gal was significantly reduced in THLE-2 cells exposed to OA/PA + H_2O_2 with rapamycin ($P <$ 0.05).

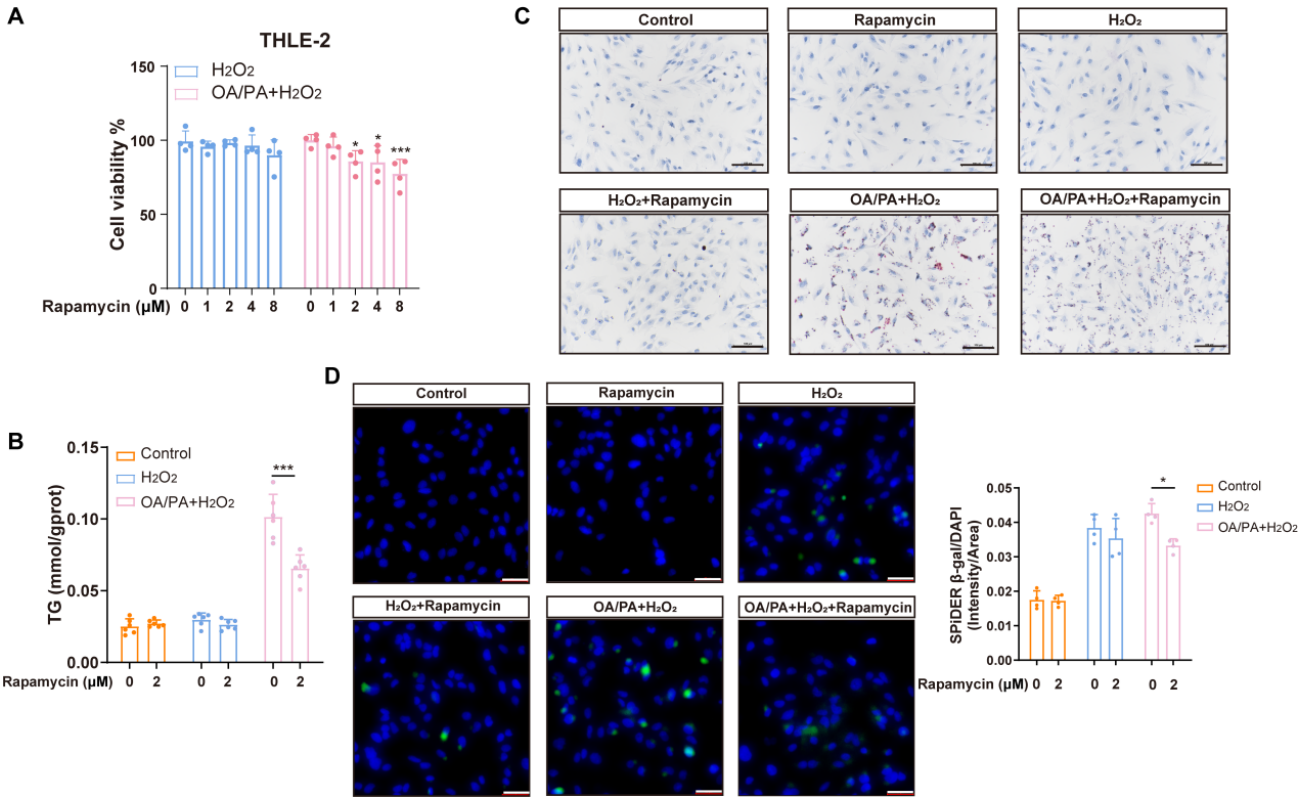

Fig 6. Lipid-lowering and anti-aging effects of rapamycin on H_2O_2-induced and OA/PA and H_2O_2-induced THLE-2 cells. (A) Effects of Rapamycin on H_2O_2-induced and OA/PA and H_2O_2-induced THLE-2 cells cell viability, and TG contents (B). (C) Representative Oil red O-stained images of THLE-2 cells. Scale bar = 100 μm. (D) Representative images of SPiDER-β-Gal staining and quantification of SPiDER-β-Gal expression. Scale bar = 100 μm. N=4 or 6, $*p < 0.05$, $**P < 0.01$, $***P < 0.001$ determined by Dunnett's test following a one-way ANOVA or Tukey's test following a two-way ANOVA.

4. Discussion

Aging leads to liver dysfunction and increased lipogenesis. Alleviating liver aging can reduce damage. Experimental models of cellular senescence, such as replicative, oncogene-induced, and stress-induced senescence, are used to study aging. H_2O_2 is often used to induce senescence in hepatocytes. However, these models lack lipid accumulation, which limits their effectiveness in simulating liver aging. Thus, an accurate and comprehensive model of hepatocyte senescence is crucial for preventing and treating aging-related liver diseases. In this study, we demonstrated that excessive lipid accumulation is one of the pathological features of liver aging. This finding is consistent with population-based cohort studies, which reported an increase in the prevalence of fatty liver disease from 35% to 51.4% among the elderly population[24-27]. To further investigate, we performed transcriptomic analysis. The fatty acid metabolic process was enriched in GO terms comparing young mice and old mice. Gene expression related to fatty acid metabolic process was markedly increased in old mice, indicating that aging is characterized by alterations in lipid metabolism. We subsequently demonstrated that significantly elevated levels of OA and PA are key indicators of liver aging via fatty acid composition analysis. These results led to the hypothesis that OA and PA accelerate liver aging through their capacity to induce steatosis and lipid accumulation in the liver[28]. Therefore, we successfully constructed a cell senescence model using OA/PA or H_2O_2 alone, and more comprehensive senescent features as well as pronounced alterations were observed in cells treated with OA/PA and H_2O_2.

H_2O_2-induced oxidative stress alone can cause senescence in hepatic cells, aligning with previous studies[29-31]. However, it fails to replicate the pronounced lipid accumulation characteristic of liver aging. By assessing various indicators of cell senescence, we propose that the combined effects of OA/PA and H_2O_2, through the induction of oxidative damage and cell cycle arrest, exacerbate the senescent phenotypes observed with application concurrently. Furthermore, transcriptomic studies on THLE-2 cells support our hypothesis by revealing that the combined treatment affects more aging-related genes, as demonstrated by the alignment of DEGs with aging hallmark genes. Meanwhile, we suspected that the DEGs that do not match may potentially serve as new markers of aging. However, the limited sample size in transcriptomic and fatty acid metabolism profiling in this study warrants caution when generalizing the identified signatures. Future studies with larger cohorts are needed for validation.

To construct a senescent model, we utilized four commonly used hepatocyte cell lines. Notably, the concurrent application of OA/PA and H_2O_2 significantly exacerbated the senescent phenotypes of AML12 and THLE-2 cells. The combined OA/PA and H_2O_2 treatment did not increase senescent cells in HepG2 and BNL CL.2 cells, as indicated by SPiDER β-gal staining, and exhibited distinct alteration trends compared to AML12 and THLE-2 cell lines. HepG2 is a human hepatocellular carcinoma cell line originating from liver tumor tissue. It is known that cancer cell lines often exhibit altered cell cycle regulation and resistance to senescence due to mutations or dysfunction in key pathways such as p53[32, 33]. Furthermore, HepG2 cells rely heavily on glycolysis which reduces their responsiveness to oxidative stress or lipid-induced mitochondrial dysfunction[34, 35]. In contrast, BNL CL.2 is a murine embryonic liver-derived cell line representing an immature and proliferative hepatic phenotype. These cells exhibit rapid proliferation, making them less susceptible to stress-induced senescence. BNL CL.2 cells also express lower baseline levels of senescence-regulatory proteins such as p16 and p21 (data not shown), further limiting their ability to model age-related oxidative damage. Our model, based on metabolic and oxidative stress, more closely mimics the pathological microenvironment in aged, steatotic livers. Primary hepatocytes or metabolically active hepatic cell lines such as AML12 or THLE-2, which retain more physiological features, are more suitable for such modeling. Therefore, the senescence phenotype observed in our model appears to be cell-type dependent, and the method is best applied to non-tumorigenic hepatocyte lines that maintain metabolic responsiveness and intact senescence signaling pathways. This study primarily focused on hepatocyte senescence induced by lipid overload and oxidative stress, reflecting a metabolic-driven model of liver aging. Accordingly, We evaluated representative markers relevant to this context, including lipid accumulation, oxidative damage, and β-galactosidase activity. However, other important features of cellular aging[36], such as mitochondrial respiratory function, the secretory profile of SASP, and the expression of senescence-associated proteins were not assessed . These aspects will be important to address in future studies to improve the comprehensiveness and biological relevance of our aging model.

After confirming the effectiveness of OA/PA combined with H_2O_2 in inducing hepatocyte senescence and exploring the transcriptomic results, we employed the anti-aging drug rapamycin to verify the reliability

of this model[37, 38]. A more pronounced phenotype was observed in the OA/PA+H_2O_2 group, reducing the probability of missed anti-aging drug discovery and improving screening efficiency. Traditional methods of inducing aging cells through oxidative stress[39, 40] and general induction methods often lack specificity. Our research focuses on liver aging and provides a more effective strategy for the discovery of anti-liver-aging drugs. This approach contrasts with conventional methods by offering a more targeted and precise way to identify potential treatments for liver aging.

However, our research focused solely on liver aging. Investigating the aging process in other organs and tissues presents an equally valuable research opportunity. Abnormal fatty acid metabolism during aging is also observed in other tissues and organs[41, 42], suggesting that fatty acids may have unexpected implications in *ex vivo* aging models when combined with other induction methods to simulate the *in vivo* aging process more comprehensively. Furthermore, since humans consume significant amounts of fatty acids daily, increased intake of fatty acids such as OA and PA throughout their lifetime may accelerate the aging process. Conversely, it is worth exploring whether supplementation with lower-fatty acid contents during aging can delay this process. Future research has emphasized the potential of food and medicine homology in addressing aging processes. The concept, rooted in Traditional Chinese Medicine (TCM), proposes that certain foods have medicinal properties, promoting health and longevity while preventing and even treating diseases[43]. Moreover, the modern transformation of food-medicine homology further integrates dietary interventions into healthcare practices, advocating for the conscious use of food therapies in preventing and mitigating aging effects, especially in liver diseases[44].

5. Conclusion

We identified abnormal fatty acid metabolism as a key characteristic of liver aging and successfully generated senescent AML12 and THLE-2 hepatic cells that accurately recapitulate many features of liver senescence in aged mice, particularly fatty acid metabolism dysfunction.

Conflict of interest

The authors declare that they have no known competing financial interests or personal relationships that could have appeared to influence the work reported in this paper.

Acknowledgments

We acknowledge BioRender (https://www.biorender.com/) for their assistance in figure creation for this study. We would like to thank the experimental conditions provided by Ganjiang Chinese Medicine Innovation Center. This work was supported by the National Natural Science Foundation of China (NSFC) (82505014), Jiangxi Provincial Natural Science Foundation (20252BAC200574), JiangXi “Double Thousand Plan” (jxsq2020101090), and the “Ganjiang Chinese Medicine Innovation Center Independent Deployment Project” (CMSC32309).

Ethics approval and consent to participate

This study was performed in line with the principles Helsinki Declaration and Basel Declaration. All animal procedures were conducted in compliance with the protocols approved by Laboratory Animal Ethics Committee of Kangtai Medical Laboratory Services Hebei Co. Ltd. (MDL2023-09-28-04).

References

1. Moon AM, Singal AG, Tapper EB. Contemporary Epidemiology of Chronic Liver Disease and Cirrhosis. Clin Gastroenterol Hepatol. 2020;18(12):2650-66.
2. Gan C, Yuan Y, Shen H, Gao J, Kong X, Che Z, et al. Liver diseases: epidemiology, causes, trends and predictions. Signal Transduct Target Ther. 2025;10(1):33.
3. Younossi ZM, Wong G, Anstee QM, Henry L. The Global Burden of Liver Disease. Clin Gastroenterol Hepatol. 2023;21(8):1978-91.
4. Wong RJ. Epidemiology of metabolic dysfunction-associated steatotic liver disease (MASLD) and alcohol-related liver disease (ALD). Metabolism and Target Organ Damage. 2024;4(4):35.
5. Yao JL, Li XX, Li MX, He YY, Sun MY, Deng QY, et al. A bibliometric analysis of lipid peroxidation in alcoholic liver disease from 2001 to 2024. Food & Medicine Homology. 2024;1:9420009.
6. Papatheodoridi AM, Chrysavgis L, Koutsilieris M, Chatzigeorgiou A. The Role of Senescence in the Development of Nonalcoholic Fatty Liver Disease and Progression to Nonalcoholic Steatohepatitis. Hepatology. 2020;71(1):363-74.
7. Maeso-Díaz R, Gracia-Sancho J. Aging and Chronic Liver Disease. Semin Liver Dis. 2020;40(4):373-84.
8. Spinelli R, Baboota RK, Gogg S, Beguinot F, Blüher M, Nerstedt A, et al. Increased cell senescence in human metabolic disorders. J Clin Invest. 2023;133(12).
9. Chikamatsu M, Watanabe H, Shintani Y, Murata R, Miyahisa M, Nishinoiri A, et al. Albumin-fused long-acting FGF21 analogue for the treatment of non-alcoholic fatty liver disease. J Control Release. 2023;355:42-53.
10. Wang W, Qian J, Shang M, Qiao Y, Huang J, Gao X, et al. Integrative analysis of the transcriptome and metabolome reveals the importance of hepatokine FGF21 in liver aging. Genes Dis. 2024;11(5):101161.
11. Reifsnyder PC, Flurkey K, Doty R, Calcutt NA, Koza RA, Harrison DE. Rapamycin/metformin co-treatment normalizes insulin sensitivity and reduces complications of metabolic syndrome in type 2 diabetic mice. Aging Cell. 2022;21(9):e13666.
12. Al-Azab M, Safi M, Idiiatullina E, Al-Shaebi F, Zaky MY. Aging of mesenchymal stem cell: machinery, markers, and strategies of fighting. Cell Mol Biol Lett. 2022;27(1):69.
13. Palmer AK, Tchkonia T, Kirkland JL. Targeting cellular senescence in metabolic disease. Mol Metab. 2022;66:101601.
14. Gao Y, Zhang W, Zeng LQ, Bai H, Li J, Zhou J, et al. Exercise and dietary intervention ameliorate high-fat diet-induced NAFLD and liver aging by inducing lipophagy. Redox Biol. 2020;36:101635.
15. Song R, Hu M, Qin X, Qiu L, Wang P, Zhang X, et al. The Roles of Lipid Metabolism in the Pathogenesis of Chronic Diseases in the Elderly. Nutrients. 2023;15(15).
16. Aravinthan A, Shannon N, Heaney J, Hoare M, Marshall A, Alexander GJ. The senescent hepatocyte gene signature in chronic liver disease. Exp Gerontol. 2014;60:37-45.
17. Lee JJ, Ng SC, Hsu JY, Liu H, Chen CJ, Huang CY, et al. Galangin Reverses H(2)O(2)-Induced Dermal Fibroblast Senescence via SIRT1-PGC-1α/Nrf2 Signaling. Int J Mol Sci. 2022;23(3).
18. Liao CM, Wulfmeyer VC, Swallow M, Falk CS, Haller H, Korstanje R, et al. Induction of Stress-Induced Renal Cellular Senescence In Vitro: Impact of Mouse Strain Genetic Diversity. Cells. 2021;10(6).
19. Almalki WH, Almujri SS. Aging, ROS, and cellular senescence: a trilogy in the progression of liver fibrosis. Biogerontology. 2024;26(1):10.
20. Childs BG, Gluscevic M, Baker DJ, Laberge RM, Marquess D, Dananberg J, et al. Senescent cells: an emerging target for diseases of ageing. Nat Rev Drug Discov. 2017;16(10):718-35.
21. Jiang X, Yang Q, Qu H, Chen Y, Zhu S. Endogenous n-3 PUFAs Improve Non-Alcoholic Fatty Liver Disease through FFAR4-Mediated Gut-Liver Crosstalk. Nutrients. 2023;15(3).

22. Gómez-Lechón MJ, Donato MT, Martínez-Romero A, Jiménez N, Castell JV, O'Connor JE. A human hepatocellular in vitro model to investigate steatosis. Chem Biol Interact. 2007;165(2):106-16.
23. Hajam YA, Rani R, Ganie SY, Sheikh TA, Javaid D, Qadri SS, et al. Oxidative Stress in Human Pathology and Aging: Molecular Mechanisms and Perspectives. Cells. 2022;11(3).
24. Chen TP, Lai M, Lin WY, Huang KC, Yang KC. Metabolic profiles and fibrosis of nonalcoholic fatty liver disease in the elderly: A community-based study. J Gastroenterol Hepatol. 2020;35(9):1636-43.
25. Riazi K, Azhari H, Charette JH, Underwood FE, King JA, Afshar EE, et al. The prevalence and incidence of NAFLD worldwide: a systematic review and meta-analysis. Lancet Gastroenterol Hepatol. 2022;7(9):851-61.
26. Hartleb M, Barański K, Zejda J, Chudek J, Więcek A. Non-alcoholic fatty liver and advanced fibrosis in the elderly: Results from a community-based Polish survey. Liver Int. 2017;37(11):1706-14.
27. Noureddin M, Yates KP, Vaughn IA, Neuschwander-Tetri BA, Sanyal AJ, McCullough A, et al. Clinical and histological determinants of nonalcoholic steatohepatitis and advanced fibrosis in elderly patients. Hepatology. 2013;58(5):1644-54.
28. Wang Y, Chen C, Chen J, Sang T, Peng H, Lin X, et al. Overexpression of NAG-1/GDF15 prevents hepatic steatosis through inhibiting oxidative stress-mediated dsDNA release and AIM2 inflammasome activation. Redox Biol. 2022;52:102322.
29. Del Mar Rivas-Chacón L, Yanes-Díaz J, de Lucas B, Riestra-Ayora JI, Madrid-García R, Sanz-Fernández R, et al. Preventive Effect of Cocoa Flavonoids via Suppression of Oxidative Stress-Induced Apoptosis in Auditory Senescent Cells. Antioxidants (Basel). 2022;11(8).
30. Kumar P, Hassan M, Tacke F, Engelmann C. Delineating the heterogeneity of senescence-induced-functional alterations in hepatocytes. Cell Mol Life Sci. 2024;81(1):200.
31. Li J, Xian L, Zheng R, Wang Y, Wan X, Liu Y. Canthaxanthin shows anti-liver aging and anti-liver fibrosis effects by down-regulating inflammation and oxidative stress in vivo and in vitro. Int Immunopharmacol. 2022;110:108942.
32. Thangavelu L, Altamimi ASA, Ghaboura N, Babu MA, Roopashree R, Sharma P, et al. Targeting the p53-p21 axis in liver cancer: Linking cellular senescence to tumor suppression and progression. Pathol Res Pract. 2024;263:155652.
33. Ozturk M, Arslan-Ergul A, Bagislar S, Senturk S, Yuzugullu H. Senescence and immortality in hepatocellular carcinoma. Cancer Lett. 2009;286(1):103-13.
34. Maseko TE, Elkalaf M, Peterová E, Lotková H, Staňková P, Melek J, et al. Comparison of HepaRG and HepG2 cell lines to model mitochondrial respiratory adaptations in non-alcoholic fatty liver disease. Int J Mol Med. 2024;53(2).
35. Xu N, Lin H, Ding X, Wang P, Lin JM. Isotope tracing-assisted chip-based solid-phase extraction mass spectrometry for monitoring metabolic changes and vitamin D3 regulation in cells. Talanta. 2025;288:127754.
36. Kroemer G, Maier AB, Cuervo AM, Gladyshev VN, Ferrucci L, Gorbunova V, et al. From geroscience to precision geromedicine: Understanding and managing aging. Cell. 2025;188(8):2043-62.
37. Partridge L, Fuentealba M, Kennedy BK. The quest to slow ageing through drug discovery. Nat Rev Drug Discov. 2020;19(8):513-32.
38. Jiang C, Tan X, Liu N, Yan P, Hou T, Wei W. Nutrient sensing of mTORC1 signaling in cancer and aging. Semin Cancer Biol. 2024;106-107:1-12.
39. Guo Y, Ayers JL, Carter KT, Wang T, Maden SK, Edmond D, et al. Senescence-associated tissue microenvironment promotes colon cancer formation through the secretory factor GDF15. Aging Cell. 2019;18(6):e13013.
40. Qi X, Ng KT, Lian Q, Li CX, Geng W, Ling CC, et al. Glutathione Peroxidase 3 Delivered by hiPSC-MSCs Ameliorated Hepatic IR Injury via Inhibition of Hepatic Senescence. Theranostics. 2018;8(1):212-22.
41. Fitzner D, Bader JM, Penkert H, Bergner CG, Su M, Weil MT, et al. Cell-Type- and Brain-Region-Resolved Mouse Brain Lipidome. Cell Rep. 2020;32(11):108132.
42. Mutlu AS, Duffy J, Wang MC. Lipid metabolism and lipid signals in aging and longevity. Dev Cell. 2021;56(10):1394-407.
43. Cong B. Perspectives in food & medicine homology. Food & Medicine Homology. 2024;1:9420018.
44. Sun-Waterhouse D, Chen XY, Liu ZH, Waterhouse GIN, Kang WY. Transformation from traditional medicine-food homology to modern food-medicine homology. Food & Medicine Homology. 2024;1:9420014.